Helium bubble formation in nuclear glass by in-situ TEM investigations

G. Gutierrez[1], S. Peuget [1,a], J.A Hinks [2], G. Greaves[2], S.E. Donnelly[2], E. Oliviero[3], C. Jégou[1]

[1] : CEA, DEN, Laboratoire d'Étude des Matériaux et Procédés Actif, 30207 Bagnols-sur-Cèze, France.

[2] : Electron Microscopy and Materials Analysis Group, School of Computing and Engineering, University of Huddersfield, Huddersfield HD1 3DH, UK.

3: Centre de Spectrométrie Nucléaire et Spectrométrie de Masse, CNRS-IN2P3, Université Paris-Sud, Orsay Campus, France.

[a)] Corresponding author: sylvain.peuget@cea.fr

ABSTRACT

The effect of helium implantation fluences in French nuclear borosilicate glass on He bubble nucleation and growth mechanisms was characterised using in-situ TEM experiments. Observations of implanted glass at 143K indicate that a helium concentration of around 3 at.% is required to nucleate a significant density of nanosized bubbles. He bubble growth is observed for He concentration higher than the estimated number of helium host (> 4 at.%). These results highlight the large capacity of the glassy network for incorporating helium atoms.

In France, fission products and minor actinides (MA) resulting from the reprocessing of spent nuclear fuel from PWR reactors are immobilized in a borosilicate matrix (known as R7T7) by vitrification. During storage, helium accumulation from alpha decay of MA will occur over time in glass. For example, the helium concentration in the glass after around 10 000 years of disposal will be around 0.03 at.% neglecting helium diffusion. In a glass package with an external environment substantially free of helium, the helium content could exceed the equilibrium concentration. As a result, helium atoms may aggregate into small clusters or bubbles that could reduce the helium mobility and induce local mechanical stress. In this context, mechanisms of helium bubble formation and growth have to be studied in order to determine whether helium bubbles can be formed under glass disposal conditions.

In oxide glasses, helium is incorporated in the glassy matrix through the glass free volume (1). Helium nucleation and growth mechanisms can be studied by two approaches: by performing thermal treatment on helium infused glasses or by generating helium by non-equilibrium methods such as implantation, irradiation in nuclear reactor using the $^{10}B(n,\alpha)^{7}Li$ reaction or by doping the glass with short half-life actinides such as ^{244}Cm or ^{238}Pu. By using the infusion method associated with a thermal treatment, Fares et al. have studied the conditions of helium bubble formation in a SON68 borosilicate glass free of radiation damage simulating the French “R7T7” nuclear waste containment glass (2). He has observed micro bubble nucleation at a concentration of 0.003 at.% as soon as the glass temperature reaches the glass vitreous transition temperature (T_G), i.e. when the glass viscosity decreases sufficiently to allow glass deformation. However, one previous work performed by Faile et al. on infused simple borosilicate glasses has exhibited bubble nucleation below T_G for higher helium content (1 at.%) (3), suggesting that a synergy between temperature and helium content could favour helium bubble formation. Moreover, the literature data concerning helium bubble formation under non-equilibrium generation methods show some discrepancies. Two studies on borosilicate glass irradiated with helium generated by the $^{10}B(n,\alpha)^{7}Li$ reaction have highlighted the bubble nucleation for irradiation temperatures below 503K

(4) and at 1023K (5). However no bubble greater than 10 nm (spatial resolution limit) was observed for an irradiation temperature lower than 343K in similar glass (6). Concerning the actinide-doped glasses, two works can be cited. Inagaki et al. have observed by SEM some pores of around 0.2 µm diameter in a Cm-doped glass of type R7T7 at a helium content of around 0.3 at.% (7). On the contrary, no pores or bubbles greater than 10 nm were observed in a SON68 curium-doped glass after the same level of alpha decay (and thus helium content (8)). The conclusions of helium implantation experiments in glasses are also contradictory. Three studies mention the possibility of bubble formation without annealing for helium concentrations of around 2 at.% (9). On the other hand, for higher helium content (3-4 at.%) another study did not reveal any bubbles (10), either by TEM or by SAXS. Finally, very recently Bes et al. have performed the first in-situ TEM helium implantation in SON68 glass and observed the nucleation of nanometer-sized bubbles at 143K at a local helium concentration of around 0.1 at.% (11). This disparity of results in the literature could be linked to several factors such as the synergetic effect of temperature, radiation damage and helium content. Moreover due to the high helium diffusivity ($D = 10.2 \pm 1.8 \times 10^{-18}$ $m^2.s^{-1}$ at room temperature (11)) it is vitally important to be very careful during each step of the experimental process (storage conditions, implantation and irradiation temperature ...). Thus in-situ experiments appear to be the best way to determine the nucleation and growth mechanisms of helium bubbles. In the present work, we have studied the effect of implantation fluence on bubble evolution using in-situ TEM investigations.

Glass samples were prepared from SON68 cylindrical rods at CEA (Marcoule, France). The glass chemical compositions are described in Ref. (12). Three foils with a 100 nm thickness were prepared for TEM observations using Focused Ion Beam (FIB) lift-off technique. TEM with in-situ ion implantation was performed using 6 keV He^+ ions with an ion beam flux up to 7.7×10^{13} ions $cm^{-2}.s^{-1}$ in the Microscope and Ion Accelerator for Materials Investigations (MIAMI) facility at the University of Huddersfield. A low implantation temperature (143K) was chosen to minimise any sample heating and

thus helium diffusion. Specimens were implanted successively at increasing fluences in the range of 0.1 to 23 x 10^{16} He.cm^{-2} corresponding to the peak concentration (at the projected range, R_p, of the implantanted ion distribution) varying from 0.1 to 23 at.% according to SRIM calculation (13). TEM observations were achieved using a JEOL JEM-2000FX TEM operating at 80 keV. Images were captured using a Gatan ORIUS SC200 camera at all fluence steps with the electron beam switched off during the implantation process in order to minimize any electron-induced glass radiation damage (11).

After implantation at 2.8 x 10^{16} He.cm^{-2} (2.8 at.% at R_p), structures of around several nm size with brighter contrast in underfocused images are observed, suggesting helium bubble nucleation. Due to the resolution limit under these observation conditions, we cannot exclude the presence of smaller bubbles (around 1-2 nm) at lower implantation fluences. The bubbles appear clearer at an implantation fluence of 4.4 x 10^{16} He.cm^{-2} as shown by the bubbles within the dotted circles in Fig. 1.a. The bubble morphology is circular with a radius of around 3 ± 1 nm. Their density is low except in some area where small bubbles are grouped along lines (arrow in Fig. 1.b). It is likely that these bubbles lines are due to a variation of the lamella thickness or of local stress that could favour helium bubble nucleation. At fluences between 4.4 and 9 x 10^{16} He.cm^{-2}, the bubbles first nucleated at low concentration remain at the same position and grow without a significant change of shape. The analysis of sequential images also highlights the presence of new bubbles with smaller sizes in areas previously free of bubbles. From a fluence of 9 x 10^{16} He.cm^{-2}, the distance between two neighbouring bubbles already formed becomes lower than 10 nm for most of the observed area inducing a modification of bubble morphology. Fig. 2 presents the bubble evolution from fluences of 9 to 23 x 10^{16} He.cm^{-2}. Observations reveal an increase of bubble density from 9 to 14 x 10^{16} He.cm^{-2}. As indicated by the dark circle on the micrographs (Fig. 2.b-d), once nucleated the bubbles remain on fixed sites and continue to grow by accumulation of implanted helium. Then when two bubbles are close enough bubble coalescence occurs inducing an evolution of the shape from circular to elongated bubbles as observed in the area illustrated by the dark arrow (Fig. 2.a-d). The smaller bubbles disappear in

favour of a bigger one. Fig. 2 also shows the presence of smaller bubbles which have formed above or the below the larger ones, the additional brightness being due to the superposition of the small and large bubbles.

Fig. 3 shows the bubble radius distributions for the samples implanted at 9, 14, 18 and 23 x 10^{16} He.cm^{-2}. 850 to 250 bubbles were counted for respectively the 9 and 23 x 10^{16} He.cm^{-2} implanted fluence. Only circular bubbles have been taking into account. At 9 x 10^{16} He.cm^{-2} a broadening of the size distribution occurs. The population of smaller bubbles (3 ± 1 nm) seen at lower concentration is still present but bubbles with bigger radius (around 8 nm) are also present. At higher fluences the mean size and the width of the bubble distribution increase with helium content. This broadening is due to bubble coalescence as observed in Fig.2.

From TEM investigations we have observed nanosized bubble nucleation at a helium concentration of 2.8 at.% (Fig. 1). It appears that a concentration around 100 times higher than the estimated helium content in the glass after around 10 000 years of disposal (0.03 at.%) is required to give rise to significant numbers of helium bubbles. In addition neither bubble diffusion nor re-solution of the helium was observed at low implantation temperature (143K). In the literature, Bes et al. observed the formation of low density helium bubbles with a radius of 1-2 nm in SON68 glass after helium implantation at lower concentration (0.1 at.%) (11). In our case, the resolution limit associated with the observation conditions (including the thickness of our FIB lamella) prevented the detection of bubbles with a radii smaller than 1 nm. However, the bubbles sizes determined are quite similar for the two in-situ studies at helium concentration of 0.1 and 2.8 at.%. As the implantation temperature and the glass composition are comparable, this indicates that the bubble size does not evolve significantly with the implantation fluence up to a helium concentration of around 3-4 at.%. However at a higher helium content (> 3-4 at.%) the bubble size increases (Fig. 3). This evolution can be correlated with the helium solubility in the glass. Indeed, a density of helium host sites (N_s) in SON68 glass of around 2.2 ± 0.6 x 10^{27} at.m^{-3} (~3 at.%) was

determined using two experimental approaches: by pressurized helium infusion at different temperatures and by ^{3}He implantation at several fluences (12). This N_s value corresponds in our case to a helium implantation fluence of 3 x 10^{16} He.cm^{-2} (3 at.%). This value fluence is close to the limiting fluence ranging from 2.8 to 4.4 x 10^{16} He.cm^{-2} where bubble growth clearly occurs. It suggests that for helium concentrations higher than N_s all host sites are occupied. Thus with increasing fluence helium atoms are unable to find any empty host sites and so accumulate inside bubbles inducing glass structure deformation and thus bubble growth. However for concentrations smaller than N_s the cavity size does not evolve significantly, only the bubble density increases. The mechanisms of nanosized bubble nucleation is not well understood at present. However several parameters seem to be involved. Indeed even at low implantation fluences, the probability for helium atoms to come to rest close to a volume already occupied by helium atoms exists and increases with the fluence. Also molecular dynamic simulations have shown that larger free volumes, with sizes sufficient to contain few helium atoms, exist inside the glass structure (14). These volumes could act as nucleation sites for the first nanosized bubbles. In addition, during the implantation process, helium atoms are introduced into the glass together with displacement cascades. The structural reorganization of glass containing helium atoms due to a collision cascade could also favour bubble nucleation. Thus the synergistic effect of radiation damage and helium content needs to be clarified in order to determine whether the implantation damage can favour bubble nucleation at low helium concentration.

This in-situ TEM He implantation study highlights the important capacity of the glassy network for accommodating large helium concentrations. On the one hand, high helium concentration is required (~3 at.%) to observe a significant density of nanosized He bubbles. On the other hand, the glassy network may be able to accommodate very high helium concentration (23 at.%) by forming a large helium bubble network without fracturing the material.

Bibliography

1. Shackelford, J. F., *Journal of Non-Crystalline Solids* **1999,** *253*, 231-241.

2. Fares, T. Comportement de l'hélium dans le verre nucléaire R7T7. Université Montpellier II, 2011.

3. Faile, S. P.; Roy, D. M., *Journal of the American Ceramic Society* **1966,** *49* (12), 638-&.

4. Sato, S.; Furuya, H.; Kozaka, T.; Inagaki, Y.; Tamai, T., *Journal of Nuclear Materials* **1988,** *152* (2-3), 265-269.

5. Malow, G. A., H. In *Helium formation from alpha-decay and its significance for radioactive waste glasses*, Scientific Basis for Nuclear Waste Management, McCarthy, G. J., Ed. Plenum Press: 1979; p 109.

6. Peuget, S., In *Private communication*, 2013.

7. Inagaki, Y.; Furuya, H.; Idemitsu, K.; Banba, T.; Matsumoto, S.; Muraoka, S., *Microstructure of simulated high-level waste glass doped with short-lived actinides, 238Pu and 244Cm*. 1992; Vol. 257, p 199-206.

8. Peuget, S.; Delaye, J. M.; Jégou, C., *Journal of Nuclear Materials* **2014,** *444* (1–3), 76-91.

9. (a) De, A. K.; Luckscheiter, B.; Lutze, W.; Malow, G.; Schiewer, E., *American Ceramic Society Bulletin* **1976,** *55* (5), 500-503; (b) Denatale, J. F.; Howitt, D. G.; Arnold, G. W., *Radiation Effects and Defects in Solids* **1986,** *98* (1-4), 63-70; (c) Terekhov, A. Y.; Heuser, B. J.; Okuniewski, M. A.; Averback, R. S.; Seifert, S.; Jemian, P. R., *Journal of Applied Crystallography* **2006,** *39*, 647-651.

10. Evron, R.; Cohen, Y.; Regev, O.; Eyal, Y.; Matzke, H.; Tinschert, K. In *Ion implantation induced microstructural damage in a nuclear waste glass*, Nuclear Society of Israel, 1994; p 18.

11. Bès, R.; Sauvage, T.; Peuget, S.; Haussy, J.; Chamssedine, F.; Oliviero, E.; Fares, T.; Vincent, L., *Journal of Nuclear Materials* **2013,** *443* (1–3), 544-554.

12. Fares, T.; Peuget, S.; Chamssedine, F.; Sauvage, T.; Bouty, O.; Broudic, V.; Deschanels, X.; Maugeri, E.; Bes, R.; Jegou, C., *Journal of the American Ceramic Society* **2012,** *95* (12), 3854-3862.

13. Ziegler, F.; Biersack, J. P.; Littmark, U., *The stopping and range of ions in matter*. Pergamon Press: New-York, 1985; Vol. 2-6.

14. Kerrache, A.; Delaye, J. M., *Nuclear Instruments and Methods in Physics Research Section B. accepted*.

Figure

Figure 1

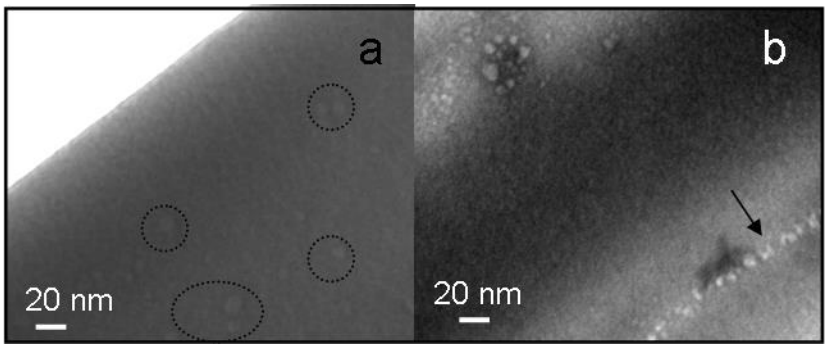

Figure 2

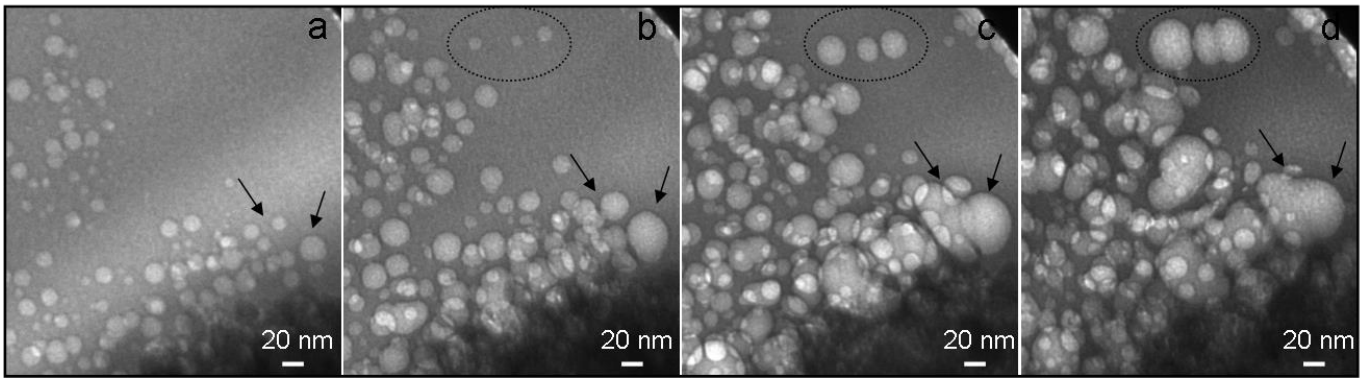

Figure 3

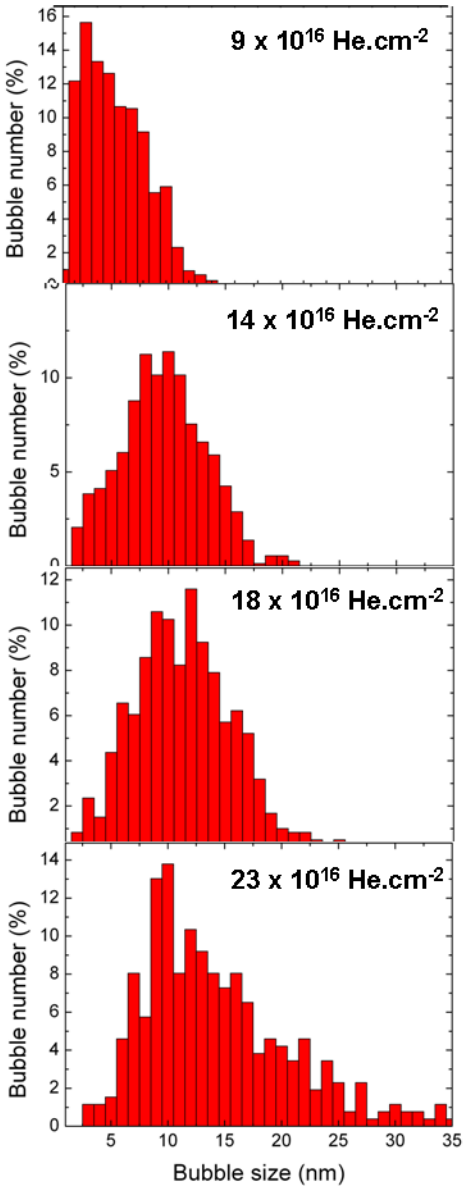
9 x 10^16 He.cm^-2
14 x 10^16 He.cm^-2
18 x 10^16 He.cm^-2
23 x 10^16 He.cm^-2
Bubble number (%)
Bubble size (nm)

Figure caption

Figure 1: TEM micrographs of SON68 glass implanted at 6 keV He ions at 143K with fluences of 4.4 x 10^{16} He.cm^{-2}. The dotted circles indicate the bubble nucleation. The arrow shows a line along which small bubbles are grouped.

Figure 2 : TEM micrographs of SON68 glass implanted at 6 keV He ions at 143K with fluences of (a) 9, (b) 14, (c) 18 and (d) 23 x 10^{16} He.cm^{-2}. The arrows show bubble coalescence with increase in helium fluence. The dotted circle indicates the nucleation and growth of bubbles.

Figure 3 : Distributions of bubbles radii, determined for glass implanted at 6 keV He ions at 143K with fluences of 9, 14, 18 and 23 x 10^{16} He.cm^{-2}. 850, 750, 600 and 250 bubbles were counted for the distributions at fluence of 9, 14, 18 and 23 x 10^{16} He.cm^{-2} respectively.